Density-functional theory study of the microstructure, electronic structure, and optical properties of amorphous carbon

Jiecai Han, Wei Gao,*,† Jiaqi Zhu,*,‡ and Songhe Meng
Center for Composite Materials, Harbin Institute of Technology, Harbin 150080, China

Weitao Zheng
Department of Materials Science, Jilin University, Changchun 130012, China
(Received 12 June 2006; revised manuscript received 20 December 2006; published 17 April 2007)

The electronic structures of amorphous carbon at densities of 2.0, 2.3, 2.6, 2.9, and 3.2 g/cm^3 have been calculated using density-functional theory with different simulation parameters. The carbon networks were generated by liquid-quench method using Car-Parrinello molecular dynamics. The sp^3 fraction and the radial distribution function are in good agreement with experimental results. At a density of 3.2 g/cm^3, the highest sp^3, content of the simulated carbon networks reaches 89%, which is the upper limit sp^3 content of the ta-C films deposited by the filtered cathodic vacuum one technique. The optical band gap increases with density (or sp^3 fraction) of the networks. The defect density of states at Fermi level can significantly reduce the optical band gap. The small rings with geometries very different from ideal sp^3 bonding cause the strong distortion of σ bond angle, which decrease the splitting of $\sigma-\sigma^*$. The distortion of π and σ bond angle can decrease the $\pi-\pi^*$ splitting. Such structural distortions can increase the states near Fermi level and reduce the optical gap.

DOI: 10.1103/PhysRevB.75.155418 PACS number(s): 61.43.Bn, 71.15.Pd, 02.70.Ns

I. INTRODUCTION

Carbon can form a variety of objects with different structural and electronic properties presented by its forms such as graphite, diamond, amorphous carbon, fullerenes, and carbon nanotubes. Amorphous carbon (*a*-C) has high mechanical hardness, elastic modulus, wear resistance, chemical inertness, infrared transparency, good biocompatibility, wide band gap, and low friction coefficient, and it can be deposited at room temperature.[1] Because of these excellent properties, the *a*-C films have many attractive applications[2] in areas such as various tools, magnetic storage, biomedical coatings, optical windows, microelectromechanical devices, and as field-emission cathode materials. Amorphous carbon films can be prepared by sputtering, mass selected ion beam, filtered cathodic vacuum arc (FCVA), and pulsed laser deposition. Usually, *a*-C containing a majority of atoms in the sp^3 configuration is referred to as tetrahedral amorphous carbon (ta-C).

Although a lot of theoretical[3–7] and experimental[8–11] efforts have been devoted to the study of this fascinating material, the understanding of its microstructure and physical properties is still far from being complete. It is a challenge to simulate *a*-C because it can form a solid specimen with twofold, threefold, and fourfold coordinations. It is still unclear whether the sp^3 fraction varies linearly with density, and how the electronic structure and optical properties depend on the microstructure. Molecular-dynamics method is a very efficient method to simulate the *a*-C structure. Much work has been done for modeling the *a*-C structure using a rapid liquid-quench method. The popular theories used to describe the interatomic interactions are density-functional theory (DFT), tight-binding approaches, and empirical potential methods.

Attempts have been made to simulate the structures of *a*-C specimen using molecular dynamics at varied accuracy, computational cost, and system size. Empirical Tersoff[12] potential is a simple yet effective technique, which is parametrized to fit the elastic constants of graphite and diamond. Kaukonen and Nieminen[13] made some progress in the simulation of the growth of diamondlike films using empirical classical many-body potential proposed by Tersoff. Kelires[14,15] also used Tersoff potential combined with Monte Carlo annealing algorithm to generate *a*-C models. Brenner[16] empirical potential works well at low densities but it appears strong deviation at high densities in modeling the *a*-C structure. Empirical environment-dependent interaction potential[17,18] (EDIP) is the most transferable among the empirical potential methods used for modeling *a*-C, which was first proposed for silicon. EDIP method shows good agreement with DFT, but it slightly underestimates the sp^3 fraction at high density.

Tight-binding molecular dynamics (TBMD) is another transferable method and can be used for realistic studies of the structure and electronic properties of *a*-C. Ho and co-workers[19–21] used TBMD to generate a range of structures with densities from 2.2 to 3.4 g/cm^3. However, the sp^3 fraction is much lower than the experimental value. Blaudeck and co-workers *et al.*[22,23] presented a density-functional-based scheme for determining the parameters of nonorthogonal tight-binding (NOTB) models. A series of carbon networks was generated with densities from 2 to 3.5 g/cm^3. The sp^3 fraction increased from 9% to 88% accordingly. Recently, Mathioudakis *et al.*[24] presented an in-depth investigation of fundamental physical trends in *a*-C based on environment-dependent tight-binding[25] simulations. They found that the variation of sp^3 fraction, or mean coordination, is linear over the whole possible range of densities. An important result is the finding of three- and four-membered rings in ta-C networks, which has never been found before except the *ab initio* simulations.

Ab initio molecular dynamics is the most accurate, trans-

ferable, and physical method. A low-density ($2\ g/cm^3$) amorphous carbon structure was first obtained based on *ab initio* molecular dynamics,[26] in which the interatomic potential is constructed directly from the electronic ground state using density-functional techniques. Then, a high-density ($2.9\ g/cm^3$) structure was generated using Car-Parrinello molecular dynamics (CPMD).[27,28] Three- and four-membered rings are first found in amorphous carbon networks, which is an unusual topology. It has not been proved yet by experiment whether such small rings exist in the ta-C structure up to now.

In this work, we performed further study on the simulation method, microstructure, electronic structure, and optical properties of *a*-C within the framework of DFT. A series of *a*-C networks with densities from 2.0 to 3.2 g/cm^3 has been generated using two different simulation parameters: pseudopotential and fictitious electronic mass. The purpose of this work is to answer the following questions.

(i) How does the microstructure depend on the density of the structure? Previous researches indicate that the sp^3 content has a linear dependence on the density of the network,[24,29,10] which may not be very religious. The sp^3 content increases as the density of *a*-C films increases in the statistical data. Strictly speaking, it is not a linear relationship, especially for high-density ta-C films.

(ii) How do the electronic structure and optical properties depend on the microstructure? We especially discuss the relationship between the small rings and their electronic structures. Atoms of three- and four-membered rings have a decrease of the $\sigma-\sigma^*$ splitting compared with other atoms, which indicates the increase of states near Fermi level and the reduction of optical band gap.

(iii) How do the simulation parameters such as pseudopotential and fictitious electronic mass (μ) influence the simulation results? Researchers have seldom discussed the influences of pseudopotential and μ on the final simulated structures. Two exchange-correlation functionals Becke-Lee-Yang-Parr[30] (BLYP) and OLYP (=OPTX+LYP) (Ref. 31) were used in this work. The simulated structures with OLYP have statistically higher sp^3 content than the structures with BLYP. Especially, at a density of $3.2\ g/cm^3$, the sp^3 content reaches 89% with OLYP, which is the upper limit sp^3 content of the ta-C films deposited by the FCVA technique.[32,10] The fictitious electronic mass (μ) is an experiential parameter and has a significant influence on the final structure, which indicates that better structures can be obtained by varying this parameter.

II. THEORETICAL CONSIDERATIONS AND COMPUTATIONAL DETAILS

All the simulation processes were implemented using *ab initio* CPMD (Ref. 33) with a plane-wave cutoff of 40 Ry and an integration time step of 3 a.u. (0.072 fs). The key to the continuous success of Kohn-Sham DFT lies in the development of improved approximations to the exchange-correlation functional (E_{xc}). Therefore, the choice of the pseudopotential becomes very important or even decisive for such complex *a*-C networks. Two exchange-correlation functionals BLYP (Ref. 30) and OLYP (=OPTX+LYP) (Ref. 31) in the Kleinman-Bylander[34] form were used in this work. BLYP is well established and has been successfully applied to *ab initio* simulations of various carbon and carbide including *a*-C.[18,29,35] OPTX is a new local exchange functional developed by Handy and Cohen.[31] Researches[36–38] showed that OLYP is similar or even superior to the well-known BLYP, with OPTX replacing the standard Becke exchange functional.

The core of the Car-Parrinello method is a novel coefficient dynamics technique, which is used to transform the electronic wave functions when the ions are moving. Car and Parrinello[39] showed that the coupling between nuclear time evolution and electronic minimization could be treated efficiently via an adiabatic dynamics approach, which indicated that the simulations strictly depend on the ability to control the drift of the electronic wave functions away from the instantaneous ground state. Therefore, an important question for CPMD is under which circumstances the adiabaticity can be achieved and how it can be controlled. Blöchl and Parrinello[40] presented a smart method to solve the problem by introducing two separate thermostats for ions and electrons without adding to the computational cost. The idea of this method is that a fictitious dynamics is introduced for electronic wave function. A very important parameter in CPMD to control the adiabatic separation is the fictitious electronic mass (μ), which is therefore also called "adiabaticity parameter." On one hand, it can determine if the molecular dynamics could work under adiabaticity; on the other hand, it can influence the final structure of simulation. The influence of μ on the modeling of *a*-C has never been discussed before. At a density of $3.2\ g/cm^3$, four μ were adopted while everything else was kept the same.

In this study, a liquid-quench technique was taken by *ab initio* CPMD within the framework of plane-wave pseudopotential DFT. There were four steps for modeling the *a*-C structure: spontaneous melting process, liquid phase equilibrating, cooling process, and solid phase stabilizing. Each simulation system contained 125 atoms in a simple cubic supercell whose volume remained constant throughout the simulation. The initial structure was a simple cubic lattice, which was highly unstable and melted spontaneously without adding any kinetic energy. Within 0.05 ps, the simple cubic lattice was destroyed, and the temperature had risen to 5000 K. Then, the liquid began to diffuse. At a temperature of 5000 K, a quench to the Born-Oppenheimer surface was performed and the system remained liquid phase at 5000 K for 0.5 ps. In the liquid equilibrating process, a Nosé thermostat[41] on both ions and electrons was applied to control the temperature of ions and the fictitious electronic kinetic energy. This thermostat prevented the electronic wave functions from drifting away from the Born-Oppenheimer surface by removing excess fictitious kinetic energy. During the cooling process, the temperature of ions was controlled by velocity rescaling algorithm, whereas the fictitious electronic kinetic energy was controlled by Nosé thermostat. The solid phases were equilibrated for another 0.5 ps by using the Nosé thermostat method to control the temperature of ions and the fictitious electronic kinetic energy.

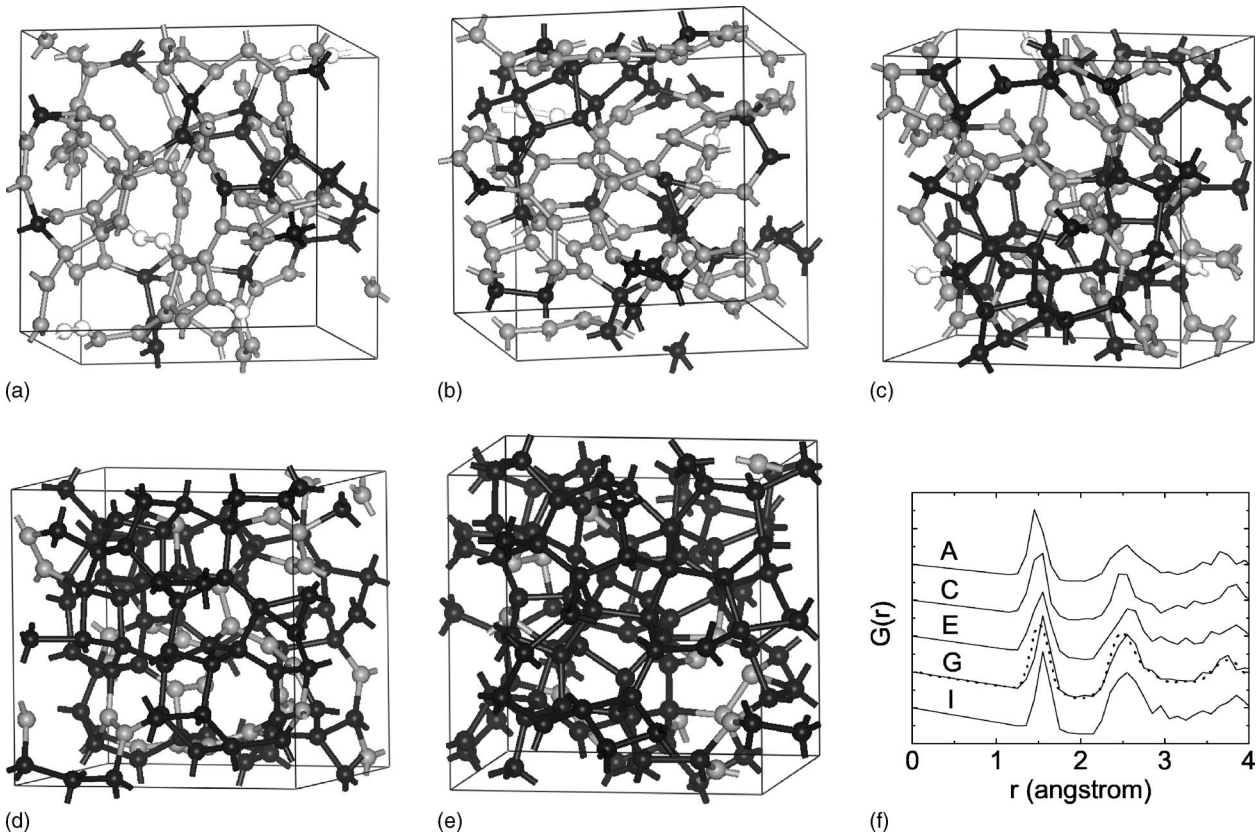

FIG. 1. Structural models of *a*-C at densities of (a) 2.0, (b) 2.3, (c) 2.6, (d) 2.9, and (e) 3.2 g/cm^3 Subfigures (a)–(e) show the carbon networks of samples A, C, E, G, and I, respectively, included in Table I. Black, gray, and white atoms denote sp^3, sp^2, and sp^1 sites, respectively. Subfigure (f) displays the radial distribution functions of samples A, C, E, G, and I (solid lines) included in Table I, compared to the neutron-diffraction data (dotted line) (Ref. 42).

III. RESULTS AND DISCUSSION

A. Structure

A series of carbon networks at densities from 2.0 to 3.2 g/cm^3 has been generated using the Car-Parrinello technique.[33] Different structures with the same density were modeled using two different exchange-correlation functionals while the fictitious electronic mass (μ) was kept 200 a.u. during the calculations. Representative carbon networks generated at 2.0, 2.3, 2.6, 2.9, and 3.2 g/cm^3 are shown in Fig. 1, while Table I summarizes some important structural properties of all the networks. As shown in Fig. 1, at a low density of 2.0 g/cm^3, the structure contains mainly sp^2-bonded atoms, sp^3-bonded atoms, and a small quantity of

TABLE I. Summary of structural parameters from the simulations in this work.

Sample	Density (g/cm^3)	E_{xc}	Bond length (Å)	Bond angle (deg)	Coordination			
					C_2	C_3	C_4	Ave
A	2.0	OLYP	1.49	115.5	5.6	75.2	19.2	3.1
B	2.0	BLYP	1.47	118.6	12	81.6	6.4	2.9
C	2.3	OLYP	1.50	113.1	3.2	64	32.8	3.3
D	2.3	BLYP	1.51	115.8	6.4	73.6	20.0	3.1
E	2.6	OLYP	1.53	112.8	2.4	52.8	44.8	3.4
F	2.6	BLYP	1.54	112.6	0	54.4	45.6	3.5
G	2.9	OLYP	1.56	110.3	0	27.2	72.8	3.7
H	2.9	BLYP	1.55	109.9	0	28.8	71.2	3.7
I	3.2	OLYP	1.56	109.2	0	11.2	88.8	3.9
J	3.2	BLYP	1.54	109.8	0	20.8	79.2	3.8

sp^1-bonded atoms with an average coordination of 3.1. Such a low-density network is open with long chains and large rings. The structure becomes more compact as the density increases. At densities above 2.6 g/cm^3, the structures contain mainly sp^3-bonded atoms without sp^1-bonded atoms involved. In a high-density 3.2 g/cm^3 network, several structures containing 77%–89% $sp3$ hybridized atoms were obtained, which are as high as that could be obtained by experiments.[10,32] Previous *ab initio* molecular-dynamics simulations[29] only generated carbon networks with about 81% sp^3 content at the same density. This difference is perhaps due to the selection of exchange-correlation functionals and different simulation parameters. With BLYP functional, the five structures at densities of 2.0, 2.3, 2.6, 2.9, and 3.2 g/cm^3 are similar to previous works[29] based on the Car-Parrinello technique. We also adopted a new exchange-correlation functional OLYP and obtained an sp^3 content which is higher than any previous work based on the Car-Parrinello technique.

The cutoff distance used to define the coordination in all the networks is 1.85 Å, which is determined from the carbon atomic radius and the radial distribution function $G(r)$ shown in Fig. 1(f). The $G(r)$ provides useful information about the simulated liquid and disordered solid which can be compared with the neutron-diffraction data. It is defined by

$$G(r) = 4\pi r[\rho(r) - \rho_0], \tag{1}$$

where $\rho(r)$ is the density of atom centers at a distance r from an atom, averaged over all atom centers in the system, and ρ_0 is the average density. The first two peaks agree well with experimental data in both the r position and the shape of the curve. Some special structures containing three- and four-membered rings were generated. Such small rings exist in all the simulated networks, which agrees with the previous *ab initio* MD simulations.[28] However, in previous works, all the atoms in the three- and four-membered rings are sp^3 hybridized. We noticed some abnormal structures that are one or two sp^2-bonded atoms existing in the three- and four-membered rings, which have been overlooked before. The most common bond angle at an sp^3 site is close to the standard tetrahedral value of 109.5° and at an sp^2 site is 120°. While three- and four-membered rings make contributions to the distribution near 60° and 90°, respectively. Such small rings decrease the average bond angle especially for the low-density structure.

As shown in Fig. 2, it seems that the sp^3 content depends on the density of the specimen as experimentally measured, and nearly linear fits of this relationship have been available.[10,24,29] Strictly speaking, the relationship is not exactly linear because the sp^3 content can vary in a range of about 10% at a given density, which depends on the deposition method and processing conditions.

B. Electronic structure and optical properties

Amorphous carbon has three kinds of hybridizations, which are mainly sp^3, sp^2, and a small quantity of sp^1 sites. sp^3 sites have only σ states while sp^2 and sp^1 sites also possess π states. σ and π states have large differences in

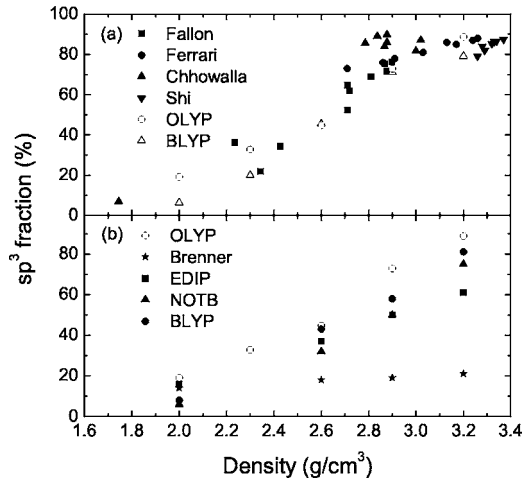

FIG. 2. The sp^3 fraction plotted as a function of density. In (a), the open circles and open up triangles are calculated from the simulation results. The solid squares (Ref. 43), solid circles (Ref. 10), solid up triangles (Ref. 44), and solid down triangles (Ref. 45) are all from experimental data. In (b), the open circles are our simulated results. Others are all from Ref. 18.

electronic structure. σ states form a network of two-center bonds between adjacent atoms. In the bond-orbital approximation, any property of occupied states such as the total energy, charge density, or polarizability can be expressed as simply the sum of independent, short-range terms for each bond. There are no long-range forces in this approximation, and the electronic structure depends on the short-range order. π states are different, because a π orbital usually interacts with π states on more than one atom to form a conjugated system such as benzene. Then, one can no longer define a unique bond orbital. Conjugated bonds cannot now be expressed as the sum of independent, two-center bonds. Each bond contains contributions from adjacent bonds, and this gives rise to long-range forces and long-range polarizabilities.[1]

Amorphous structures are significantly different from crystal structures in electronic states. The electronic states in an amorphous system are either extended or localized. In amorphous carbon, states in the middle of bands and states next to the band edge called "tail states" are localized. The localized and extended states are separated by an energy called the mobility edge. The band gap is no longer a perfectly forbidden gap but contains some localized states. The mobility gap is defined as the energy difference between the valence- and conduction-band mobility edges. The optical band gap is an energy difference between the density of states (DOS) at the conduction- and valence-band edges. In a-Si:H, the definitions of E_{04} gap, Tauc gap, and mobility gap are all closely the same value, which is not the case in a-C:H or ta-C. In contrast, the E_{04} gap in a-C:H or ta-C is always nearly 20% higher than the Tauc gap.[1] The mobility gap is much wider than the optical gap because the optical gaps are controlled by the DOS only. The optical matrix element does not depend on localization. The strong localization of states in a-C has a significant effect on the electronic properties and devices, as it lowers the carrier mobility.[46]

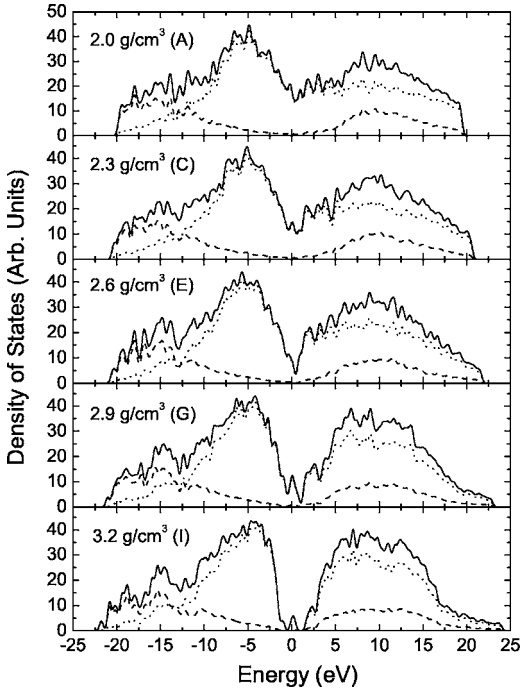

FIG. 3. The electronic density of states of the simulated structures A, C, E, G, and I included in Table I. The solid line is the total DOS of the *s* and *p* orbitals. The dotted and dashed lines correspond to projections of the *p* and *s* orbitals, respectively.

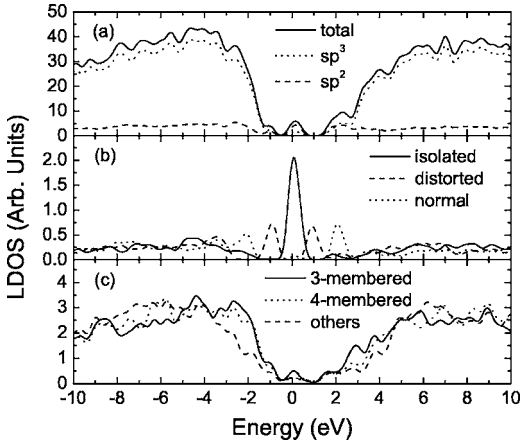

FIG. 4. The calculated local density of states for sample I. In (a), the solid line is the total DOS of all atomic orbitals, while the dotted and dashed lines correspond to projections of sp^3 and sp^2 hybridized orbitals. In (b), the LDOS of three kinds of typical sp^2 atoms are compared. In (c), the LDOS of nine atoms with sp^3 hybridized orbitals which belong to three-membered rings, four-membered rings, and others (not belong to small rings).

The DOS and optical properties were calculated using the CASTEP code,[47] which is based on DFT using Vanderbilt-type ultrasoft pseudopotentials[48] and a plane-wave expansion of wave functions. We used the generalized gradient approximation (GGA) in the scheme of Perdew-Burke-Ernzerhof[49] to describe the exchange and correlation potential, since the GGA is more accurate than the local-density approximation. The computed total and projected densities of states of the five simulated structures at different densities were shown in Fig. 3. The Fermi level is set to 0 eV. A Gaussian curve with a standard deviation of 0.2 eV has been used to smoothen the data. As would be expected, there are states near Fermi level in all the simulated structures. The states near Fermi level decrease in intensity as the density increases. The local density of states (LDOS), which was shown in Fig. 4(a), indicates that the states near Fermi level are mainly from the contributions of sp^2 hybridized atoms. This could explain why the structure with a high sp^3 fraction has lower states near Fermi level.

The electronic properties of the ta-C films are controlled by π and π^* states, which lie close to Fermi level, whereas the mechanical properties are controlled by σ and σ^* states. Therefore, we are mainly interested in π and π^* states in this work. The defects have the most important influence on the reduction of the optical gap, because in the case of a dangling bond, a peak is obtained at Fermi level. Experimental results[50–53] indicate that defects can reduce the optical gap of *a*-C (*a*-C:H) quite a lot. Teo *et al.*[54] obtained the highest optical gap ta-C by vacuum annealing to decrease defects while maintaining a high sp^3 fraction. Another important factor for the determination of the effective optical gap is the smallest π-π^* splitting which occurs with non-negligible abundance. Our simulated models do not support the presence of aromatic rings even in low-density *a*-C, because the fivefold, sixfold, and sevenfold rings are strongly cross-linked by the inclusion of at least one or two sp^3 atoms. Here, we are more concerned about high-density ta-C. In our simulated ta-C structures, there are only short sp^2 chains and dimer sp^2 atoms. The defects are isolated sp^2 atom and odd numbered sp^2 chains. The LDOS of such a defect is shown in Fig. 4(b) (solid line). The LDOSs of normal dimer sp^2 atoms indicate that the π-π^* splitting is about 4 eV. If an sp^2 site lies in a strongly distorted network, the bond angle of π and σ will be far from normal values, where the π-π^* splitting will reduce to about 2 eV, as shown in Fig. 4(b) (dashed line), which indicates the increase of states near Fermi level and the reduction of optical gap.

Besides the sp^2 atoms, we also investigated some special sp^3 atoms, which have a slight influence on the band, edge. As shown in Fig. 4(c), atoms of three- and four-membered rings have a decrease of σ-σ^* splitting compared with other atoms. In other structures, the small rings have the same contribution to the DOS. The decrease of σ-σ^* splitting has a slight influence on the optical gap because the σ-σ^* splitting is much higher than the π-π^* splitting. So, the optical gap is mainly determined by sp^2 atoms. However, such small rings have an influence on valence- and conduction-band tails and thus have an influence on the optical band edge.

It is well known that the interaction of a photon with the electrons in the system can be described in terms of time-dependent perturbations of the ground-state electronic states. Transitions between occupied and unoccupied states, including plasmons and single particle excitations, are caused by the electric field of the photon. The spectra resulting from these excitations can be described as a joint density of states between the valence and conduction bands. The imaginary part $\varepsilon_2(\omega)$ of the dielectric function can be calculated from the momentum matrix elements between the occupied and

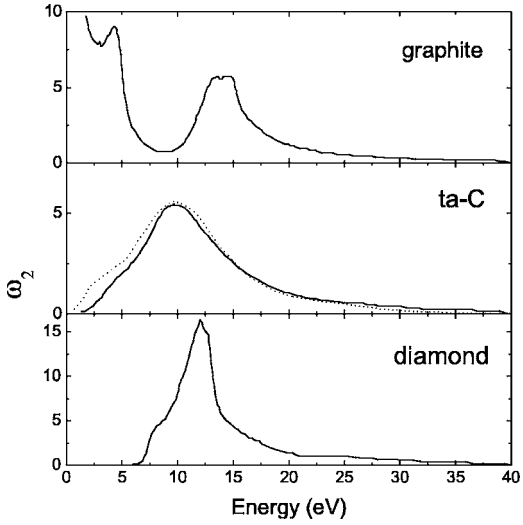

FIG. 5. The calculated ε_2 spectra (dotted line) of sample L compared with experimental data (Ref. 55) of graphite, diamond, and ta-C.

unoccupied wave functions within the selection rules, and the real part $\varepsilon_1(\omega)$ of dielectric function can be evaluated from imaginary part $\varepsilon_2(\omega)$ by Kramers-Kronig relationship. Thus, absorption coefficient $\alpha(\omega)$ can be derived from equationn

$$\alpha(\omega) = \sqrt{2}\omega[\sqrt{\varepsilon_1^2(\omega) + \varepsilon_2^2(\omega)} - \varepsilon_1(\omega)]^{1/2}. \quad (2)$$

Figure 5 shows the comparison of the ε_2 spectra of diamond, graphite, ta-C film obtained by experiment, and calculated ε_2 spectra of ta-C. The ε_2 spectra of graphite show two peaks, one around 4 eV due to π excitations and one about 13 eV due to σ excitations. Diamond shows only a single peak at 13 eV due to σ excitations. Low-density ta-C with low sp^3 fraction shows two peaks, one weak peak at around 4 eV due to π-π^* transitions, the other at 9–11 eV due to σ-σ^* transitions. The ta-C with high sp^3 fraction has only one main peak at around 10 eV due to σ-σ^* transitions. Our calculations accord well with the experimental results. The peak position in ta-C (about 10 eV) is lower than in diamond (13 eV) because the loss of the k-selection rule in amorphous solids allows transitions to occur at lower energy.[55] In addition, the structural distortions such as small rings would also reduce the σ-σ^* transitions as described above, which could be another explanation.

As is typical for amorphous materials, it is difficult to measure the band gap from the DOS due to the presence of states near Fermi level. A useful measurement of the optical gap can be obtained by calculating the E_{04} gap or Tauc gap using the imaginary part of the dielectric permittivity $\varepsilon_2(\omega)$. The process of calculating $\varepsilon_2(\omega)$ for the simulated structure is a straightforward one involving a convolution of the occupied and unoccupied densities of states, provided one makes the assumption that matrix elements for dipole transitions are independent of energy. The optical-absorption characteristics of the simulated structures are plotted in Fig. 6. Usually, the Tauc gap is obtained by the linear fraction of the curve.

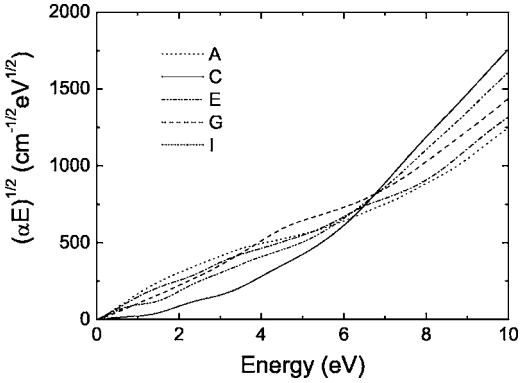

FIG. 6. The optical-absorption characteristics of the simulated structures A–I.

Because the calculated results do not show good linearity, we only calculated the E_{04} gaps for comparison with the experimental data, as shown in Fig. 7. The calculated E_{04} gaps are 0.43, 0.49, 0.92, 1.51, and 3.23 eV for the samples A (2.0 g/cm^3), C (2.3 g/cm^3), E (2.6 g/cm^3), G (2.9 g/cm^3), and I (3.2 g/cm^3), respectively. The calculated E_{04} gaps are lower than experiments because of the inherent limitation of DFT.

C. Simulation parameters

Two simulation parameters investigated in this work are exchange-correlation functional and fictitious electronic mass (μ). μ is an intrinsic part reflecting the experimental deposition process and are not artifacts of the simulation technique. Exchange-correlation functional deals with the accuracy of simulation. The simulation results show that the structures with OLYP compare better with experiments than the structures with BLYP at five different densities at least for the sp^3 content. The simulated structures with BLYP have a slightly lower sp^3 fraction than the experimental data. This confirmed previous researches[36–38] that OLYP is similar or even superior to the well-known BLYP. In addition to the sp^3 fraction, the average bond length, bond angle, and the distri-

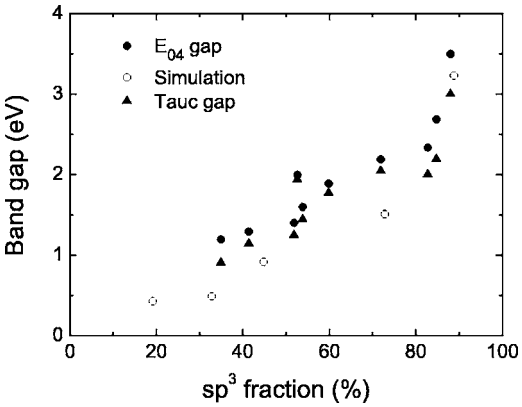

FIG. 7. The optical band gap of the simulated structures and experimental results. Open circles denote the calculated E_{04} gaps of samples A, C, E, G, and I. Solid circles and solid triangles are experimental data (Refs. 44 and 54).

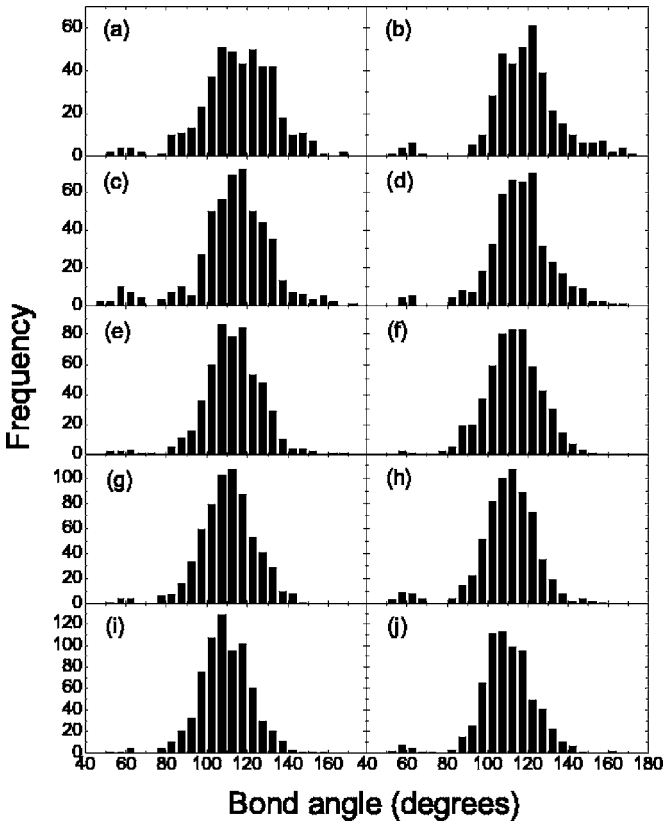

FIG. 8. Bond angle distributions of the simulated structures. Subfigures (a)–(j) stand for samples A–J included in Table I.

butions of bond angles are also different, as shown in Table I and Fig. 8. With OLYP and BLYP, the bond angle distributions larger than 140° have a general reductive tendency with increasing density. The bond angle distributions near 60° and 90° have an obvious reductive tendency with increasing density with OLYP, while the tendency is not obvious with BLYP.

The Car-Parrinello technique differs from other *ab initio* molecular-dynamics methods by the dynamical optimization method for the electronic wave-function degrees of freedom (i.e., the basis set expansion coefficients) which can be treated simultaneously with the Newtonian nuclear dynamics. The parameter of inertia, usually called "fictitious electronic mass," controlling the response of the basis set coefficients to the potential in the simulated annealing approach, is chosen much more than real electronic mass and much

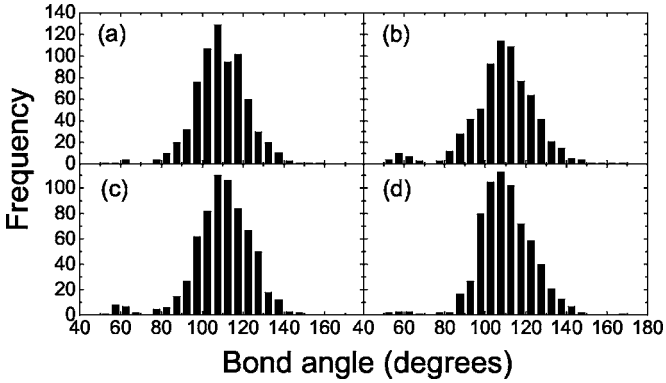

FIG. 9. Bond angle distributions of the simulated structures. Subfigures (a), (b), (c), and (d) stand for samples I, K, L, and M, respectively, included in Table II.

smaller than the atomic masses. In this way, the wave function adapts instantaneously to the moving nuclei, keeping the electrons sufficiently close to the ground state. For a given physical system, the only parameter to control adiabatic separation is the fictitious mass, which is therefore also called "adiabaticity parameter." If μ is too small, eventually the time step appears too large and the integration by the Verlet algorithm is not correct anymore, which gives rise to a drift in the constant of motion. So, the reduction of μ has the drawback that the time step needs to be reduced. Thereby, it will decrease the computational efficiency of the method. If μ is too large, electrons are too heavy and adiabacity will be lost. As a consequence, we have to make a compromise. And μ is a parameter determining not only the adiabaticitiy issues but also the dynamic process. It can be seen from Table II and Fig. 9 that μ has a large influence on the simulated structures.

IV. CONCLUSION

The structures of amorphous carbon with different simulation parameters at densities of 2.0, 2.3, 2.6, 2.9, and 3.2 g/cm^3 have been modeled using *ab initio* molecular dynamics. The microstructure, electronic structure, optical properties, and their relations were investigated. The simulated structures with OLYP have statistically higher sp^3 content than the structures with BLYP. At a density of 3.2 g/cm^3, the sp^3 content reaches 89% with OLYP, which is the upper limit sp^3 content of the ta-C films deposited by the

TABLE II. Summary of structural parameters from the networks produced with different μ. All of the four samples were generated with OLYP.

Sample	μ	Bond length (Å)	Bond angle (deg)	Coordination			
				C_2	C_3	C_4	Ave
I	200	1.56	109.2	0	11.2	88.8	3.9
K	300	1.54	108.9	0	11.2	88.8	3.9
L	400	1.53	109.7	0	23.2	76.8	3.8
M	500	1.54	110.0	0	20.8	79.2	3.8

FCVA technique.[10,32] The fictitious electronic mass (μ) is an experiential parameter and has a large influence on the final structure, which indicates that researchers can obtain better structures by adjusting this parameter. The optical gap increases with increasing density (or sp^3 fraction) of the networks. The small rings with geometries very different from ideal sp^3 bonding cause the strong distortion of σ bond angle, which decrease the splitting of σ-σ^*. The distortion of π and σ bond angle has a noticeable decrease of π-π^* splitting. Such structural distortions would increase the states near Fermi level and reduce the optical gap. The defects such as isolated sp^2 sites and odd numbered sp^2 chains will give a state at Fermi level, which significantly reduce the optical gap.

ACKNOWLEDGMENTS

We would like to thank C. Q. Sun for his valuable comments and suggestions. This work was supported by National Natural Science Foundation of China (Grant No. 50602012).

*Corresponding authors.
†Electronic address: gw_hit@hit.edu.cn
‡Electronic address: zhujq@hit.edu.cn

[1] J. Robertson, Mater. Sci. Eng., R. **37**, 129 (2002).
[2] Y. Lifshitz, Diamond Relat. Mater. **8**, 1659 (1999).
[3] Y. Lifshitz, S. R. Kasi, and J. W. Rabalais, Phys. Rev. Lett. **62**, 1290 (1989).
[4] D. R. McKenzie, D. Muller, and B. A. Pailthorpe, Phys. Rev. Lett. **67**, 773 (1991).
[5] B. Zheng, W. T. Zheng, S. S. Yu, H. W. Tian, F. L. Meng, Y. Wang, J. Zhu, S. H. Meng, X. D. He, and J. C. Han, Carbon **43**, 1976 (2005).
[6] K. J. Koivusaari, T. T. Rantala, and S. Leppävuori, Diamond Relat. Mater. **9**, 736 (2000).
[7] H. U. Jäger and K. Albe, J. Appl. Phys. **88**, 1129 (2000).
[8] J. Schwan, S. Ulrich, T. Theel, H. Roth, H. Ehrhardt, P. Becker, and S. R. P. Silva, J. Appl. Phys. **82**, 6024 (1997).
[9] A. C. Ferrari and J. Robertson, Phys. Rev. B **61**, 14095 (2000).
[10] A. C. Ferrari, A. Libassi, B. K. Tanner, V. Stolojan, J. Yuan, L. M. Brown, S. E. Rodil, B. Kleinsorge, and J. Robertson, Phys. Rev. B **62**, 11089 (2000).
[11] K. J. Koivusaari, T. T. Rantala, J. Levoska, and S. Leppävuori, Appl. Phys. Lett. **76**, 2794 (2000).
[12] J. Tersoff, Phys. Rev. Lett. **61**, 2879 (1988).
[13] H. P. Kaukonen and R. M. Nieminen, Phys. Rev. Lett. **68**, 620 (1992).
[14] P. C. Kelires, Phys. Rev. B **47**, 1829 (1993).
[15] P. C. Kelires, Phys. Rev. Lett. **73**, 2460 (1994).
[16] D. W. Brenner, Phys. Rev. B **42**, 9458 (1990).
[17] N. A. Marks, Phys. Rev. B **63**, 035401 (2001).
[18] N. A. Marks, N. C. Cooper, D. R. McKenzie, D. G. McCulloch, P. Bath, and S. P. Russo, Phys. Rev. B **65**, 075411 (2002).
[19] C. Z. Wang, K. M. Ho, and C. T. Chan, Phys. Rev. Lett. **70**, 611 (1993).
[20] C. Z. Wang and K. M. Ho, Phys. Rev. Lett. **71**, 1184 (1993).
[21] C. Z. Wang and K. M. Ho, Phys. Rev. B **50**, 12429 (1994).
[22] T. Frauenheim, P. Blaudeck, U. Stephan, and G. Jungnickel, Phys. Rev. B **48**, 4823 (1993).
[23] U. Stephan, T. Frauenheim, P. Blaudeck, and G. Jungnickel, Phys. Rev. B **50**, 1489 (1994).
[24] C. Mathioudakis, G. Kopidakis, P. C. Kelires, C. Z. Wang, and K. M. Ho, Phys. Rev. B **70**, 125202 (2004).
[25] M. S. Tang, C. Z. Wang, C. T. Chan, and K. M. Ho, Phys. Rev. B **53**, 979 (1996).
[26] G. Galli, R. M. Martin, R. Car, and M. Parrinello, Phys. Rev. Lett. **62**, 555 (1989).
[27] N. A. Marks, D. R. McKenzie, B. A. Pailthorpe, M. Bernasconi, and M. Parrinello, Phys. Rev. Lett. **76**, 768 (1996).
[28] N. A. Marks, D. R. McKenzie, B. A. Pailthorpe, M. Bernasconi, and M. Parrinello, Phys. Rev. B **54**, 9703 (1996).
[29] D. G. McCulloch, D. R. McKenzie, and C. M. Goringe, Phys. Rev. B **61**, 2349 (2000).
[30] C. Lee, W. Yang, and R. G. Parr, Phys. Rev. B **37**, 785 (1988).
[31] N. C. Handy and A. J. Cohen, Mol. Phys. **99**, 403 (2001).
[32] X. Shi, L. K. Cheah, J. R. Shi, Z. Sun, and B. K. Tay, J. Phys.: Condens. Matter **11**, 185 (1999).
[33] Computer code CPMD (Car-Parrinello molecular dynamics), copyright IBM Corp., 1990–2001, copyright MPI für Festkörperforschung, Stuttgart, 1997–2005 (http://www.cpmd.org).
[34] L. Kleinman and D. M. Bylander, Phys. Rev. Lett. **48**, 1425 (1982).
[35] A. R. Merchant, D. R. McKenzie, and D. G. McCulloch, Phys. Rev. B **65**, 024208 (2001).
[36] W. M. Hoe, A. J. Cohen, and N. C. Handy, Chem. Phys. Lett. **341**, 319 (2001).
[37] J. Baker and P. Pulay, J. Chem. Phys. **117**, 1441 (2002).
[38] X. Xu and W. A. Goddard, J. Phys. Chem. A **108**, 40 (2004).
[39] R. Car and M. Parrinello, Phys. Rev. Lett. **55**, 2471 (1985).
[40] P. E. Blöchl and M. Parrinello, Phys. Rev. B **45**, 9413 (1992).
[41] S. Nosé, J. Chem. Phys. **81**, 511 (1984).
[42] K. W. R. Gilkes, P. H. Gaskell, and J. Robertson, Phys. Rev. B **51**, 12303 (1995).
[43] P. J. Fallon, V. S. Veerasamy, C. A. Davis, J. Robertson, G. A. J. Amaratunga, W. I. Milne, and J. Koskinen, Phys. Rev. B **48**, 4777 (1993).
[44] M. Chhowalla, J. Robertson, C. W. Chen, S. R. P. Silva, C. A. Davis, G. A. J. Amaratunga, and W. I. Milne, J. Appl. Phys. **81**, 139 (1997).
[45] S. Xu, B. K. Tay, H. S. Tan, L. Zhong, Y. Q. Tu, S. R. P. Silva, and W. I. Milne, J. Appl. Phys. **79**, 7234 (1996).
[46] C. W. Chen and J. Robertson, J. Non-Cryst. Solids **230**, 602 (1998).
[47] M. D. Segall, P. J. D. Lindan, M. J. Probert, C. J. Pickard, P. J. Hasnip, S. J. Clark, and M. C. Payne, J. Phys.: Condens. Matter **14**, 2717 (2002).
[48] D. Vanderbilt, Phys. Rev. B **41**, 7892 (1990).
[49] J. P. Perdew, K. Burke, and M. Ernzerhof, Phys. Rev. Lett. **77**, 3865 (1996).
[50] N. M. J. Conway, A. Ferrari, A. J. Flewitt, J. Robertson, W. I. Milne, A. Tagliaferro, and W. Beyer, Diamond Relat. Mater. **9**, 765 (2000).
[51] S. Schutte, S. Will, H. Mell, and W. Fuhs, Diamond Relat. Mater.

2, 1360 (1993).

[52] S. Xu, M. Hundhausen, J. Ristein, B. Yan, and L. Ley, J. Non-Cryst. Solids **164**, 1127 (1993).

[53] G. Fanchini, A. Tagliaferro, D. P. Dowling, K. Donnelly, M. L. McConnell, R. Flood, and G. Lang, Diamond Relat. Mater. **9**, 732 (2000).

[54] K. B. K. Teo, A. C. Ferrari, G. Fanchini, S. E. Rodil, J. Yuan, J. T. H. Tsai, E. Laurenti, A. Tagliaferro, J. Robertson, and W. I. Milne, Diamond Relat. Mater. **11**, 1086 (2002).

[55] S. Waidmann, M. Knupfer, J. Fink, B. Kleinsorge, and J. Robertson, J. Appl. Phys. **89**, 3783 (2001).